EPJ Photovoltaics **12**, 8 (2021)

https://doi.org/10.1051/epjpv/2021008

Available online at:
www.epj-pv.org

REGULAR ARTICLE OPEN ACCESS

High efficiency perovskite solar cells using DC sputtered compact TiO_2 electron transport layer

Ahmed Hayali[1,2,*] and Maan M. Alkaisi[1,2]

[1] Department of Electrical and Computer Engineering, University of Canterbury, Christchurch, 8041, New University of Canterbury, Christchurch, New Zealand
[2] The MacDiarmid Institute for Advanced Materials and Nanotechnology, Wellington 6140, New Zealand

Received: 2 March 2021 / Received in final form: 20 October 2021 / Accepted: 26 October 2021

Abstract. High conductivity and transparency of the electron-transporting layer (ETL) is essential to achieve high efficiency perovskite solar cells (PvSCs). Generally, titanium dioxide (TiO_2) has been extensively utilized as an ETL in PvSCs. Both surface roughness and uniformity of the compact-TiO_2 (C-TiO_2) can influence the efficiency of the PvSC. This work investigates the optimization of the direct current (DC) sputtering power and the ratio of argon (Ar) to oxygen (O_2) plasma to achieve high quality ETL films. The effect of changing the DC sputtering power on the C-TiO_2 films and subsequently on the overall efficiency was studied. The electrical and optical properties of the C-TiO_2 layer were characterized for various DC powers and different ratios of Ar to O_2 plasma. It was found that the optimum preparation conditions for the C-TiO_2 films were obtained when the DC power was set at 200 W and a flow rate of 6 sccm Ar and 12 sccm O_2. A power conversion efficiency (PCE) of 15.3% in forward sweep and 16.7% in reverse sweep were achieved under sunlight simulator of 100 mW/cm^2. These results indicate that significant improvement in the efficiency can be achieved, by optimizing the C-TiO_2 layer.

Keywords: Electron transport layer / DC sputtering / compact TiO_2 / high efficiency perovskite solar cells

1 Introduction

Due to the continued global energy demands, alternative energy sources that are sustainable and less harmful to the environment are being explored. The organic-inorganic hybrid perovskite solar cells (PvSCs) have been first developed in 2009 with conversion efficiency of 4% [1]. One decade later, it has reached an efficiency of over 25% [2]. The efficiency of PvSCs has been continuously improving by employing different materials for both the active layer and electron and hole transport layers as well as different fabrication techniques. Researches have been focused on how to improve the composition of the perovskite film to yield high quality crystal structure [3], and how to improve the stability and PCE [4,5]. Although there are noticeable improvements in the PvSCs performance, its stability and reproducibility are still impeding market penetration and their wide scale commercialization. Generally, both the ETL and the hole transport HTL layers forms an interfacing layers in PvSCs. The organic inorganic perovskite layer is sandwiched between the cathode (ETL), and anode (HTL) layers [6,7]. Thus, those interface layers are essential in any effort to improve the performance of the PvSCs. One of the critical layers that can determine the photovoltaic performance of the PvSCs is the ETL. The ETL plays a central function in transferring electrons to the external electrodes and blocking the backflow of the holes at the same time. Therefore, it is worth optimise the ETL and understand its effects on cell stability and efficiency. Although there are a number of materials such as SnO_2, ZnO that can be utilized as an ETL, most of the ETL materials are based on the titanium oxide (TiO_2) due to its good conductivity and high transparency. For example, a typical value of the SnO_2 transparency is about 90% and its conductivity is around 600 S/cm at room temperature [8]. Whereas, the transparency of the TiO_2 is 90% over the visible range with much higher conductivity of 2.2×10^4 S/cm [9].

In addition to C-TiO_2, mesoporous TiO_2 (M-TiO_2) is one of most widely used ETL for the PvSCs, it has good stability, high transparency, excellent optoelectronic properties, and short deposition processes [10]. In addition, the M-TiO_2 layer can block holes and collect electrons because of its large surface area and ability to extract electrons by improving the interface layer [11]. Moreover,

* e-mail: ahmed.hayali@pg.canterbury.ac.nz

an effective balance between the flux of holes and electrons can be achieved using the M-TiO_2. The effective balance between holes and electronics flow in the mesoporous structured PvSCs has resulted in less current-voltage hysteresis compared with other types of the ETL. However, the transmission path of electrons in the C-TiO_2 layer is much shorter than in the M-TiO_2 layer [12]. Improved performance of the PvSCs can be achieved by optimising the ETL to prevent critical carrier recombination at the interfaces.

Liu et al. has proposed using Li-doped C-TiO_2 layer and achieved PCE of 17% [11]. A number of studies reported on the optimisation and improvements of the C-TiO_2 layer to enhance the efficiency of the PvSCs [10,13,14]. However, most of these methods are complicated and require high temperature treatment. For example, Saliba et al. in 2018 [15] demonstrated a 20% efficiency of PvSCs by using C-TiO_2 prepared using aerosol spray pyrolysis and lithium salt doping of the M-TiO_2. This technique requires high temperature treatment by holding the sample at 450 °C for 1 h. Another attempt in the same year, Sidhik et al. has studied the effect of using cobalt as doping for the M-TiO_2, resulting in efficiency of 18% [16]. The ETL in their study consisted mainly of two layers. The first layer was a blocking TiO_2 and the second layer was M-TiO_2 treated with different concentrations of FK209. This method required two high temperature treatments, the first by holding the sample at 500 °C for 1 hour and the second annealing the sample at 450 °C for 30 min.

Recently in 2021, Jeong et al. has reported on perovskite solar cells with power conversion efficiency of 25.6%, these cells have long-term operational stability (450 h) and show intense electroluminescence with external quantum efficiencies of more than 10%. Their ETL was prepared using high temperature process; "Prior to the spraying process, the FTO substrates were placed on a hot plate and the temperature was increased to 450 °C rapidly. After the spray pyrolysis step, the substrates were stored at 450 °C for 1 h and then slowly cooled to room temperature. The FTO/C-TiO_2 substrates prepared with m-TiO_2 were heated at 500 °C on a hot plate for 1 h to remove organic compounds first, and then slowly cooled to 200 °C" [2].

In the present work, DC-sputtering was used to deposit the C-TiO_2. The DC-sputtering is a well establish technique employed for high throughput scalable manufacturing environment. It is a low temperature processing, which does not require holding the sample at elevated temperatures as compared with the aerosol spray pyrolysis of C-TiO_2 deposition method. Moreover, the perovskite film reported by Sidhik et al. was based on $MAPbI_3$ ($CH_3NH_3PbI_3$) [16]. We report here on Cesium Lead Iodide $CsI_{0.05}[(FAPbI_3)_{0.85}\ (MAPbBr_3)_{0.15}]_{0.95}$ based perovskite films.

There is no study, to our knowledge, that reported on the use of C-TiO_2 deposited by DC-sputtering with the M-TiO_2 layer as an ETL. A combined C-TiO_2 and cobalt FK209 doped M-TiO_2 were used as an ETL. Both cobalt FK209 doped M-TiO_2 were spun coated after the deposition of C-TiO_2. The effect of different DC sputtering powers and ratios of argon (Ar) to oxygen (O_2) plasma during the deposition of the C-TiO_2 were investigated. Finally, the influence of preparation conditions on the J_{sc}, V_{oc}, FF, and PCE of PvSCs were observed. Furthermore, the reproducibility and stability of the cell were improved compared with other deposition methods.

2 Experimental details

2.1 Materials

All basic materials were supplied commercially and were utilized as received without any extra purification. Conductive Soda Lime glass fluorine-doped tin oxide (FTO, 12–15 Ω/sq) was sourced from MSE pro^{TM} supplies. Titanium dioxide (TiO_2) paste (30NR-D), formamidinium iodide (FAI), and methylammonium bromide (MABr) were procured from greatcell solar. Lead (II) iodide (PbI_2) 99.9%, and lead (II) bromide ($PbBr_2$) 99.9% were purchased from luminescence technology corp. (Lumtec). Bis(trifluoromethane)sulfonimide lithium salt (Li-TFSI 99.9%), acetonitrile anhydrous, (99.8%), spiro-MeOTAD 99% (HPLC),chlorobenzene (95%),tris(2-(1H-pyrazol-1-yl)-4-tert-utylpyridine)cobalt(III)tri[bis(trifluoromethane)sulfoni- mide] FK209 Co(III) TFSI salt and 4-tert-Butylpyridine (TBP 98%) were bought from Sigma-Aldrich. Caesium iodide (CsI 99.998%) was purchased from alfa aesar. N, N-dimethylformamide (DMF, 99.5%) and dimethyl sulfoxide (DMSO, 99.9%) were acquired from Fisher Scientific.

2.2 Solar cell fabrication

2.2.1 Substrate preparation

In this work, a commercially available FTO (FTO, 12–15 Ω/sq) glass substrate was utilized. Practically, the glass substrate coated with FTO was etched one-third of its total area to allow for front contact formation. The zinc powder (Sigma-Aldrich) and dilute hydrochloric acid (2 M) diluted in deionized (DI) water were mixed as an etching for the FTO coated substrate to avoid short circuits during the characterization of the cell. Substrates were cleaned in the ultrasonic bath using acetone, methanol, and isopropanol for 10 min, 15 min, 5 min respectively. Finally, the substrates were dried with pure nitrogen and kept in the oven for 1 h at 100 °C. Oxygen plasma Asher was used for 10 min to clean and remove any residual organic particles on the substrates. This is to improve the adhesion between the FTO and subsequent layers.

2.2.2 Preparation of electron transport layers (ETL)

Two main layers were used in this work as an ETL, a C-TiO_2 and M-TiO_2. Firstly, the C-TiO_2 layer was deposited using DC- sputtering with a titanium target (3" diameter × 0.25" thick and 99.995% purity). The DC-sputtering source is powered by 200 W and the process plasma were a mixture of Argon (Ar) and Oxygen (O_2) with flow rates of 6 and 12 standard cubic centimetres per minute (sccm) respectively. The C-TiO_2 film was deposited onto the FTO substrate with thicknesses between 60 and 70 nm forming an amorphous TiO_2 film. The second layer is called the mesoporous TiO_2 (M-TiO_2), which was prepared by using 150 mg of TiO_2 paste (30N-RD) dissolved in 1 mL of

Table 1. Main materials used to prepare the perovskite precursor.

Chemical name	Symbol	Company Name	Molar ratio	Molecular weight
Formamidinium iodide	FAI	DYE SOL	1 mole	171.97 mg/mole
Methylammonium bromide	MABr	DYE SOL	0.2 mole	111.97 mg/mole
Lead iodide	PbI_2	Lumtec	1.1 mole	461.9 mg/mole
Lead bromide	$PbBr_2$	Lumtec	0.2 mole	367.01 mg/mole
Caesium iodide	CsI	Lumtec	1.5 mole	259.809 mg/mole

ethanol. This liquid mixture is stirred vigorously overnight at temperature of 70 °C. Doping of M-TiO_2 was obtained by adding cobalt Fk209 salt to further enhance the electronic transport layer properties. The doping solution was prepared by mixing cobalt (2.5 mg) with acetonitrile (200 µL) then added to the M-TiO_2 solution. Cobalt doped M-TiO_2 was deposited by spin coating resulted in 150 nm thick films based on setting the spinner at a speed of 4000 rpm with 2000 rpm/s acceleration for 10 s. After finishing the spin coating process, the film was dried for a few minutes by preheating at 100 °C on hot plate. The temperature was increased gradually to 125 °C then held the samples for 5 min. The heating cycle was repeated by increasing the temperature to 375 °C for 15 min and held for 5 min. Finally, increasing the temperature to 450 °C then keep samples on the hot plate for 30 min to form an anatase phase during the annealing process. All the annealing processes were performed at the laboratory ambient. Practically, a glass lid was used to cover the samples on the hot plate during the whole annealing process to enable a more temperature uniformity distribution over the substrate. Once the above process is finished, the samples were left on the hot plate to gradually cool down to 125 °C before moving them to the glove box to deposit the perovskite layer at room temperature. The samples were kept in a pure nitrogen circulated glove box.

2.2.3 Perovskite solar cell fabrication

The temperature inside the glove box was kept between 21 and 27 °C as higher temperatures above 28 °C might affect the quality of perovskite layer. Temperatures higher than 28 °C during film preparation is known to influence the crystallization of perovskite [17], and thus might affect the perovskite film quality [15]. The active perovskite layer was prepared by a method described elsewhere [18]. Table 1 shows the main materials used to prepare the perovskite precursor.

Principally, anhydrous dimethylformamide (DMF) and dimethyl sulfoxide (DMSO) were prepared by the volume ratio of DMF: DMSO 4:1 (v:v).The chemical formula of the perovskite material used in this study is $CsI_{0.05}[(FAPbI_3)_{0.85}(MAPbBr_3)_{0.15}]_{0.95}$. Using the concentration in Table 1, the solution precursor was prepared. The CsI is prepared by dissolving 1.5 M of CsI in DMSO. Hence, a 5% ratio of the C_SI was added to the total precursor to attain the required "triple-cation composition" [18]. The final stock of (5% C_SI and solution of perovskite precursor) inside the glovebox was deposited by two steps spin coating: first step, was dropping 100 µL of final stock on the sample (TiO_2 covered sample), then using a low spinning speed of 1000 rpm for 10 s to ensure full surface coverage. A second step uses a high speed 6000 rpm spinning for 25 s was followed. After 15 s, a 220 µL of chlorobenzene (CBZ) was quickly poured by pipet in the middle of the 2.5 × 2.5 cm^2 sample ten seconds before the end of the spinning. This step is critical as longer or shorter times can results in poor quality films. As a result, both of (DMSO/DMF) have been removed from the substrate by CBZ during spin coating. After finishing the preparation process, perovskite film seems semi-transparent and was annealed at 100 °C for 40–50 min.

2.2.4 Hole transport layer (HTL) and backside electrode

The HTL was prepared by dissolving 80 mg of spiro-MeOTAD (Sigma-Aldrich) in 1mL of CBZ. Then adding 29 µL of 4-tert-butylpyridine (TBP) to the spiro-MeOTAD mixture. A 520 mg of lithium salt bis (trifluoromethane) sulfonimide was dissolved in 1 mL of acetonitrile, and a 300 mg of cobalt salt (FK209) salt was dissolved in 1 mL of acetonitrile. Finally, adding 18 µL of Li salt TFSI and 30 µL of cobalt salt (FK209) to the stock solution of spiro-MeOTAD as additives. A 100 µL of the final stock solution is deposited at the beginning of the spinning rotation at 4000 rpm for 20 s. This layer should look homogeneously distributed and smooth over the sample area due to using dynamic deposition method. Then, 70 nm of gold was deposited by electron beam evaporator as the electrodes. In this work, a shadow mask (heat resistance paper) was used to form a pattern of Au electrode onto the cell. Figure 1 illustrates the schematic for PvSCs fabrication procedure followed in this work.

2.3 Device and measurement characterization

Figure 2 illustrates the main structure of the PvSC device and a picture of the perovskite cell fabricated in this work. Current density–voltage (J–V) characteristic curves of the PvSCs were obtained by employing a sunlight simulator (ABET Sun3000) AM 1.5G (100 mW/cm^2) illumination. The overall sample size is 2.5 × 2.5 cm^2. The active device area used to calculate the efficiency is defined by the back gold contact area of 0.36 cm^2. The rest of the device was masked with black tape. The number of samples used for each experiment was at least 10.

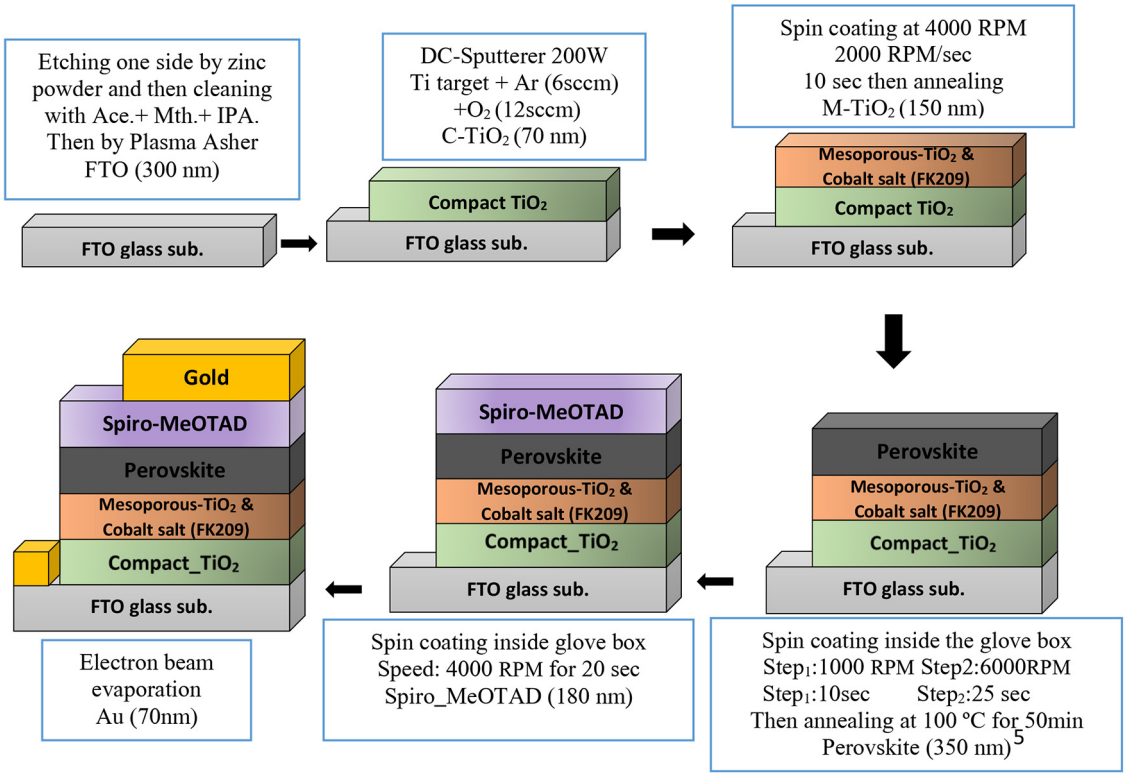

Fig. 1. Schematic steps for the fabrication procedure followed to construct the PvSCs. The compact TiO_2 was DC sputtered in an Ar/O_2 plasma. The perovskite is prepared inside a N_2 atmosphere glove box.

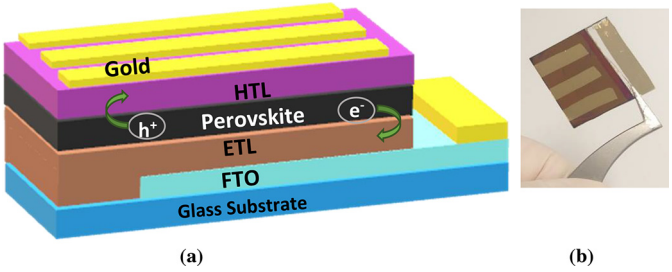

Fig. 2. (a) Schematic structure of the PvSC and (b) photo of the perovskite cell fabricated in this work.

The cross-section of the sample was obtained using scanning electron microscope (SEM) based on a Raith-150 EBL machine. Atomic force microscope (AFM) digital instruments (Veeco Instruments Inc. DI 3100) and the Raith SEM were used to characterize the morphology of the C-TiO_2. Cary 6000i ultraviolet-visible spectrometer was utilized to measure the C-TiO_2 layer absorbance and transparency versus wavelength.

3 Results and process discussion

3.1 Structure properties of compact TiO_2

To understand the influence of the C-TiO_2 on the performance of the PvSCs, the C-TiO_2 film was deposited using DC-sputtering at different powers. Four film layers prepared with different DC powers (180, 200, 220 and 240 watt) were deposited on FTO substrate and studied. The electrical and electronic properties of these layers were measured using van-der-Pauw four-probe method. It can be seen from Table 2 that the conductivity of the C-TiO_2 sputtered at 200 W is higher than other layers sputtered at different DC powers. Besides, the mobility of the C-TiO_2 layer sputtered at 200 W is also higher compared with the other preparation conditions. The conductivity of the C-TiO_2 sputtered at 200 W was measured for samples prepared at different ratios of Ar and O_2. It can be noticed from Table 3 that the optimum ratio of Ar and O_2 is equal to 6 and 12 sccm respectively. This optimum ratio of Ar/O_2 achieved high conductivity value of 1.6×10^3 [S/cm] and lower resistivity of 6.15×10^{-4} [Ω.cm].

Since the properties of the C-TiO_2 layer play a significant role in the overall performance of the PvSCs, the C-TiO_2 surface topography were investigated with AFM and SEM imaging. Figure 3 shows the surface of the C-TiO_2 sputtered at 200 W has denser grains as compared with samples sputtered at (180, 220, 240) watts. Furthermore, the C-TiO_2 film sputtered at 200 W resulted in a smoother surface and was more homogeneous compared with other layers. This is demonstrated by the low surface roughness of the "root mean square" (RMS). The surface roughness value of the C-TiO_2 sputtered at 200 W is 17 nm, which is lower than films deposited at different DC powers.

Table 2. Electrical properties of the compact TiO_2 prepared with different DC powers measured using the van-der-Pauw four-probe method.

Name	Conductivity (σ) [S/cm]	Bulk resistivity (ρ) [Ω.cm]	Mobility (μ) [cm^2/v s]
Compact TiO_2 (180 W)	9.64×10^2	1.03×10^{-3}	5772.8
Compact TiO_2 (200 W)	1.624×10^3	6.15×10^{-4}	5429.6
Compact TiO_2 (220 W)	1.16×10^3	8.6×10^{-4}	1316.6
Compact TiO_2 (240 W)	1.25×10^3	7.99×10^{-4}	873.86

Table 3. Electrical properties of the compact TiO_2 fabricated with different ratios of Ar/O_2 plasma measured using the van-der-Pauw four-probe method.

Name	Conductivity (σ) [S/cm]	Bulk resistivity (ρ) [Ω.cm]	Mobility (μ) [cm^2/v s]
C-TiO_2 (200 W) Ar(6) O_2(6)	902.35	1.1×10^{-3}	1,272
C-TiO_2 (200 W) Ar(6) O_2(12)	1,624	6.15×10^{-4}	5,429.6
C-TiO_2 (200 W) Ar(12) O_2(6)	66.33	1.507×10^{-2}	1,802.3
C-TiO_2 (200 W) Ar(12) O_2(12)	183.44	5.45×10^{-3}	6,229.2

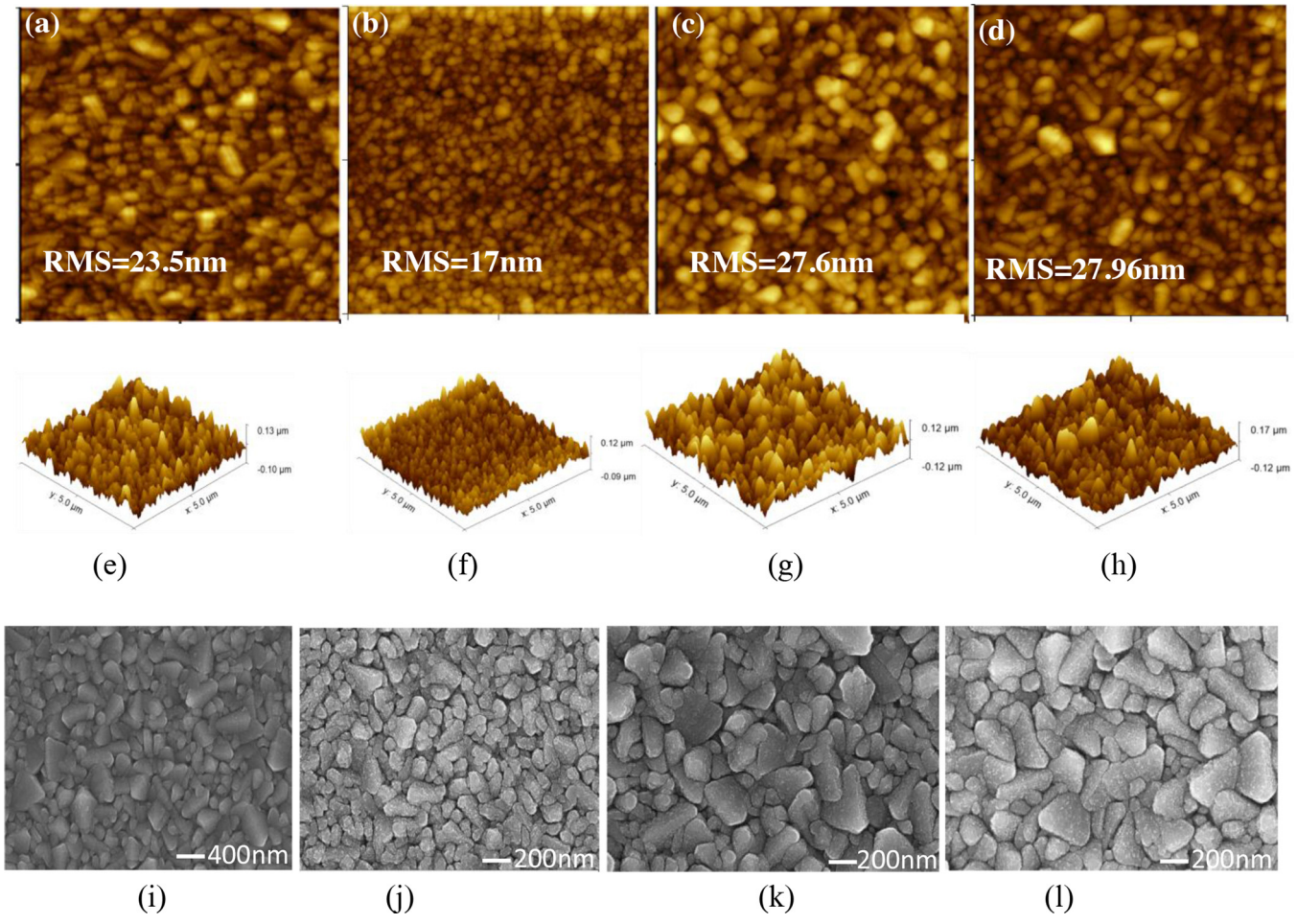

Fig. 3. Surface topographic structure of the compact TiO_2, so films were grown by DC-sputtering with different powers. Using AFM scanning two and three dimensions for (a,e) 180 W, (b, f) 200 W, (c, g) 220 W and (d, h) 240 W. In addition, showing changing grains size of C-TiO_2 using SEM scanning for (i) 180 W, (j) 200 W, (k) 220 W and (l) 240 W. AFM images were $5 \times 5\,\mu m^2$ scale.

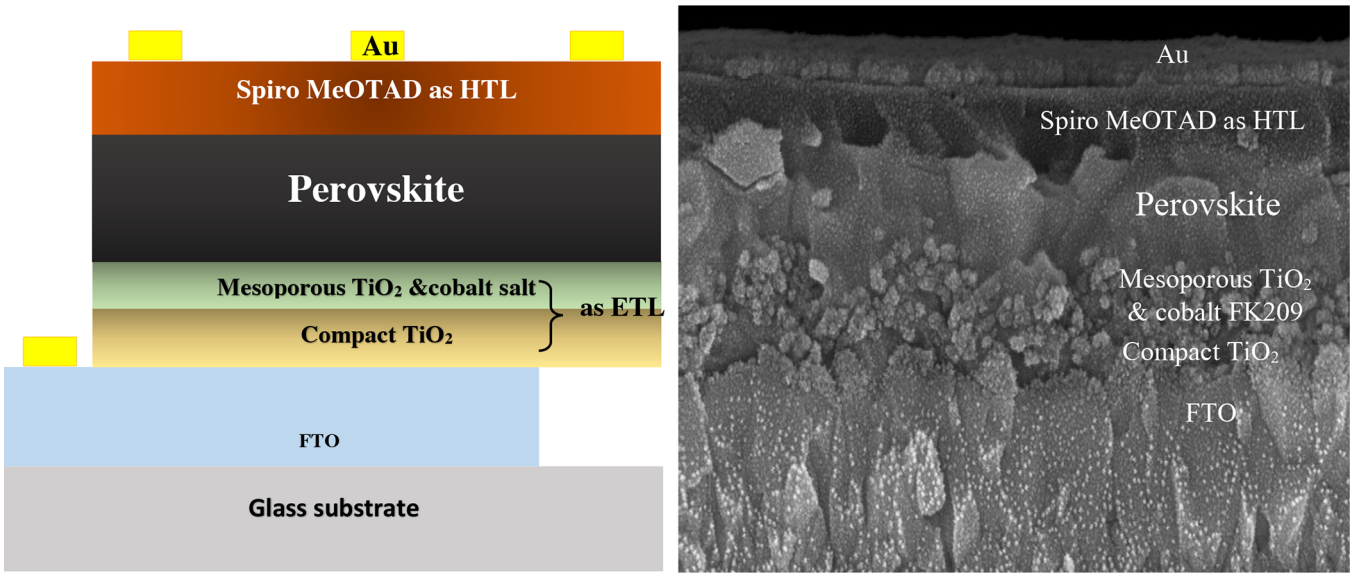

Fig. 4. (a) Schematic structure of the fabricated PvSC (2-D), and (b) an SEM image of the cross section of the device fabricated in this work.

It is found that the C-TiO_2 sputtered at 200 W gave improved performance as it provided smother interface with the M-TiO_2 layer. The AFM and SEM images in Figure 3 show that grains size of the DC sputtered C-TiO_2 film powered at 200 W is smaller than the grains size of the other layers. Based on the C-TiO_2 powered at 200 W, grain sizes between 100–400 nm were obtained with an average size of 250 nm.

Figure 4 illustrates an SEM image of the cross section of the fabricated PvSC. The different layers stack architecture is illustrated as labelled for a complete device composed of (FTO/C-TiO_2/M-TiO_2 + FK209/Perovskite active layer $CsI_{0.05}[(FAPbI_3)_{0.85}(MAPbBr_3)_{0.15}]_{0.95}$/spiro-MeOTAD, and the Au electrode. The optimized perovskite solar cell comprises of a 70 nm thick C-TiO_2 layer, a 150 nm thick cobalt FK 209 doped M-TiO_2 film. The active perovskite layer thickness is averaged at 350 nm, a 180 nm thick spiro-MeOTAD, and finally a 70 nm of the electron beam evaporated gold as electrodes for the solar cell.

3.2 Current–voltage characterization

All current voltage characteristics were conducted using (ABET Sun3000) sunlight simulator at AM 1.5G and an average light intensity of 100 mw/cm^2. Samples were 2.5 × 2.5 cm^2 in size with an average active area of 0.36 cm^2 and measurements were taken at room temperature of 21–27 °C. The active area is defined by the area of the window opening on the otherwise masked backside of the glass substrate. Measured value of the active device area is 0.36 cm^2 which is larger than most of the reported areas in the literatures [12–16]. The cells were exposed to simulated sunlight through this window. Furthermore, we are using FTO glass substrate with sheet resistance of 12–15 Ω/sq. When all of these factors were taken into considerations, the average forward and reverse scan of J_{sc} were 24.5 mA/cm^2. This is consistent with the highest J_{sc} obtained with PvSC [2].

All the results discussed in this study were conducted on active area of 0.36 cm^2, however, for comparison, cells with active area of 0.5 cm^2 and 1 cm^2 were also fabricated. The forward and reverse scan efficiency of the 0.5 cm^2 and 1 cm^2 were 15%, 16.5% and 11.5%, 12.1% respectively. The efficiency of the 1 cm^2 device is considerably lower than the 0.36 cm^2 device due to increased defect density, however, scaling up is beyond the scope of this work. An Abet technology model 15150 reference cell with KG5 filter traceable to NIST, NREL, Fraunhofer ISE and ISPRA standard artefacts were employed to certify our efficiency measurements. The full characterisation of the reference cell is given in the supplementary section.

Figure 5 displays the (J–V) characteristic curves of the PvSCs based on C-TiO_2 DC sputtered at (180, 200, 220, 240) watt. All fabrication parameters of the PvSC including the DC powers used for the deposition of the C-TiO_2 are shown in Table 4. It is demonstrated that the PvSCs based on sputtered C-TiO_2 and cobalt doped M-TiO_2 as an ETL achieved the highest efficiency with an average PCE of 16%. The measurement was repeated a few times and averaged with resulting current density (J_{sc}) of 24.5 mA/cm^2, fill factor (FF) of 61.4% and open-circuit voltage (V_{oc}) of 1021 mV. The C-TiO_2 layer deposited using DC sputtering at 200 W gave the highest efficiency of 15.3% in the forward and 16.7% in the revers scan compared to solar cells prepared at other DC powers. The PCE has improved by 17% in forward scanning and 11% in backward scanning for the C-TiO_2 sputtered at 200 W compared to the C-TiO_2 sputtered at 240 W. There is an increase of about 19% in forward scan and 6% in reverse

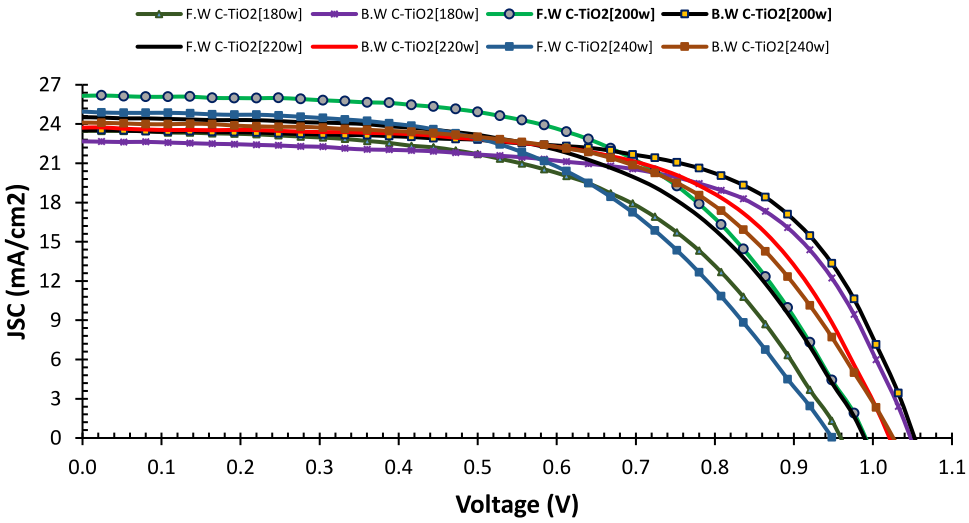

Fig. 5. J–V characteristic curves of the fabricated PvSC based on C-TiO_2 DC sputtered at 180, 200, 220, and 240 watts.

Table 4. Perovskite solar cell key parameters measured for C-TiO_2 DC sputtered films at 180, 200, 220, and 240 watts at Ar (6 sccm) and O_2 (12 sccm). Where an averaged efficiency of 16% was obtained at 200 W.

Sample description	Sweep direction	EFF%	FF%	V_{oc} [mV]	J_{sc} [mA/cm^2]	V_{max} [mV]	J_{max} [mA/cm^2]	I_{sc} [mA]	R_{shunt} [Ω]	R_{series} [Ω]
Compact- TiO_2 Based on 180W	Forward	12.8	55.5	959	23.1	668	18.7	8.3	3748	30
	Backward	15.7	64	1047	22.3	808	18.9	8.09	3632	22
Compact- TiO_2 Based on 200W	Forward	15.3	57.4	991	25.8	696	21	9.3	4069	27
	Backward	16.7	65.5	1052	23.3	808	20.1	8.4	13990	18
	Average	16	61.4	1021	24.5	752	20.7	8.85	9029	22
Compact- TiO_2 Based on 220W	Forward	14.7	57	989	24.2	696	19.9	8.7	78027	28
	Backward	16	62.4	1021	23.3	752	20.1	8.4	6451	24
Compact- TiO_2 based on 240W	Forward	13	53	949	24.7	612	20.4	8.9	2518	39
	Backward	15	59	1026	23.8	752	19.5	8.6	11595	31

scan in PCE for C-TiO_2 sputtered at 200 W compared with the C-TiO_2 sputtered at 180 W. This is in agreement with the resistivity decrease in layers deposited at different powers as shown in Table 2. The variations in short circuit current density were small between samples and, averaged around 24 mA/cm^2 in forward and backward scanning but it has dropped to about 22 mA/cm^2 for C-TiO_2 sputtered at 180 W. The V_{oc} is maintained at about 1 V for all types in the forward scanning, and was more than 1 V in the backward scanning. The FF has improved by 3.4% and 8.3% in forward scanning and 2.3% and 11% in backward scanning for the C-TiO_2 prepared at 200 W compared to the C-TiO_2 sputtered at 180 W and 240 W respectively. The combination of the DC sputtered compact TiO_2 ETL with the Cesium Lead Iodide $CsI_{0.05}$ $[(FAPbI_3)_{0.85}(MAPbBr_3)_{0.15}]_{0.95}$ based perovskite offered the potential for scaling up and resulted in a more reproducible cells with good stability [16]. In addition, we attribute this improvement in PCE to the drop in the resistivity of the C-TiO_2 sputtered at 200 W layer comparing to others as shown in Table 2.

3.3 Optical properties of compact TiO_2

Figure 6a shows transparency of FTO glass covered with C-TiO_2 having a thickness of 70 nm. It is worth noting that the C-TiO_2 has approximately the same transparency as the bare FTO glass. It is clear that the transparency of the C-TiO_2 prepared with different DC powers has more than 90% transparency over the visible wavelength range. Figure 6b presents the absorbance of the C-TiO_2 measured using Ultraviolet-Visible spectrometry (Cary 6000i). From the curves shown in Figure 6 there is a weak absorption between 350 and 800 nm, and much higher absorption between 250 and 350 nm in accordance with the expected absorption spectra for TiO_2.

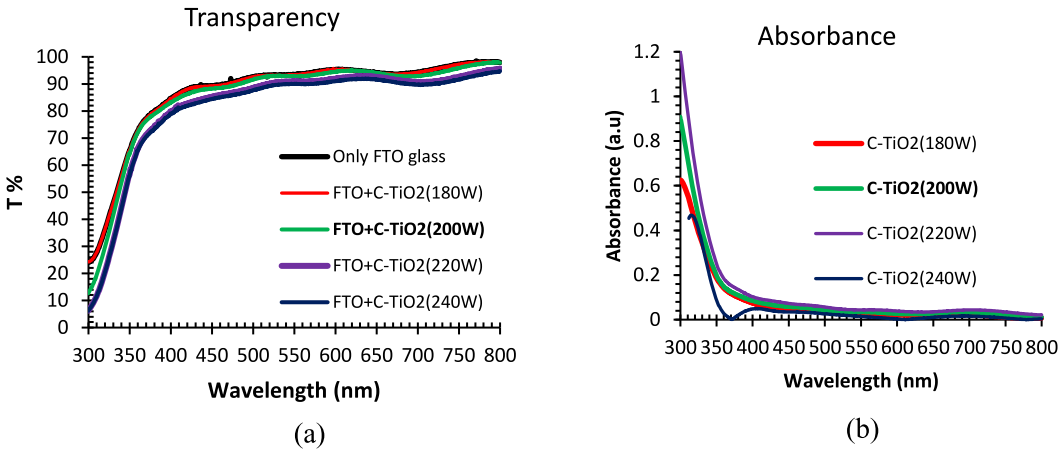

Fig. 6. Optical properties of C-TiO_2 coated FTO glass (a) transparency of the FTO glass without and with a C-TiO_2 prepared with different sputtering powers (b) absorbance spectrum of C-TiO_2 sputtered with different powers.

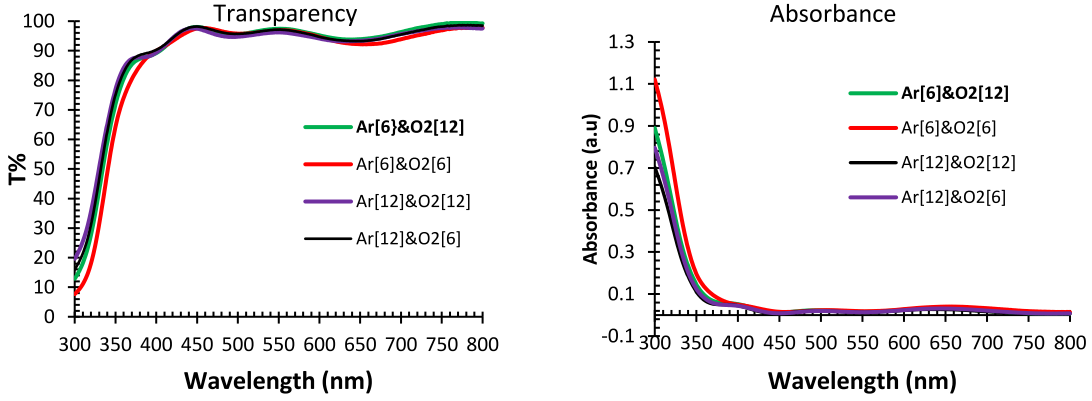

Fig. 7. Optical properties of C-TiO_2 coated FTO glass prepared at different ratios of Ar and O_2 (a) transparency (b) absorbance.

Figure 7 shows that the highest transparency was achieved when of the ratio of O_2 to Ar was 6 to 12 sccm.

3.4 Stability and reproducibility of the perovskite solar cell

To examine the reproducibility of our process, we have prepared a total of 20 solar cells all with DC sputtered C-TiO_2 layers. Ten samples were fabricated using DC sputtering powered at 200 W and 5 samples at each of the other DC powers. The stability of the fabricated devices were studied by measuring the solar cell parameters (EFF%, FF%, V_{oc}, J_{sc}, V_{max}, J_{max}, I_{sc}, R_{shunt}, and R_{series}) under sunlight simulator condition (AM 1.5G [100 mW/cm^2] using [ABET Sun3000] and was monitored over 70 days period. Figures 8 and 9 illustrate the forward and reverse scan efficiency measurements conducted over the length of 10 weeks in two different atmospheres, in a vacuum held dissector (Fig. 8) and in laboratory ambient (Fig. 9).

The drop in efficiency was from 2% to 5% during the 70 days period measured at one week intervals. Ten samples were tested for stability studies and some samples were kept in a desiccator and compared with samples kept in laboratory ambient for stability measurements. The average drop for all samples was 3.4%. Not all of the samples efficiency dropped at the same rate, so the figure below shows the variation in efficiency as measured weekly.

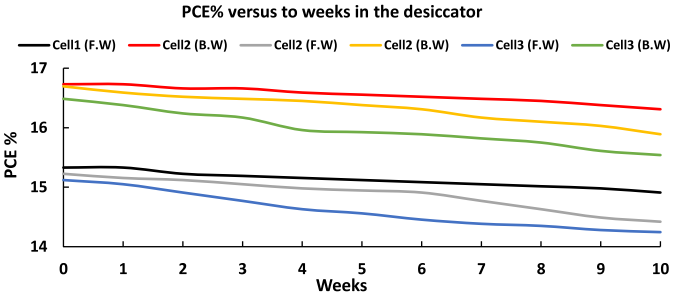

Fig. 8. Variations in the efficiency of the perovskite solar cells measured over 70 days period in weekly intervals. Devices were kept in controlled desiccator for this part of the stability testing.

As prepared efficiency of champion device in the forward and reverse scanning were 15.3% and 16.7% respectively. Four weeks later, the efficiency in the forward and reverse scanning dropped to 15% and 16.5%

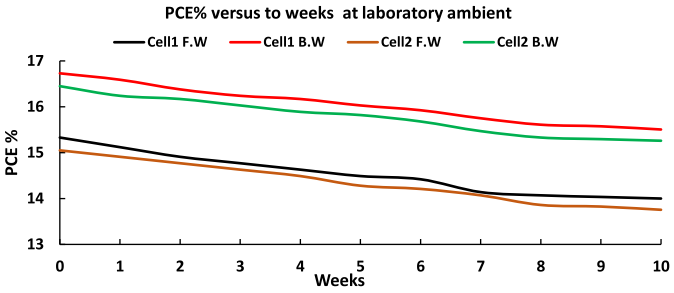

Fig. 9. Variations in the efficiency of the perovskite solar cells measured over 70 days period in weekly intervals. Devices were kept in laboratory ambient.

respectively. After eight weeks, the efficiency in the forward and reverse scanning was about 14.6% and 16% respectively. The percentage of drop in efficiency is maintained over the 70 days period the test was conducted. We did not observe any large variations in the efficiency or variations from sample to sample when prepared under same conditions an indication that the use of DC sputtered compact TiO_2 offer greater reproducibility and stability compared to other techniques. However, samples stored in ambient condition exhibit more percentage drop in efficiency of 7% as compared to those kept in a dissector were an average of 3.4% drop is measured in agreement with the trend observed in perovskite based solar cells.

4 Conclusion

We have investigated the role of DC power and the Ar to O_2 ratio in sputtered TiO_2 to form compact TiO_2 layer suitable for high efficiency perovskite solar cells. An optimum sputtering condition to obtain the desired TiO_2 layer was found to be 200W DC power with Ar (6 sccm) and O_2 (12 sccm). The cobalt doped M-TiO_2 were deposited on C-TiO_2 to further improve the electron transport layer (ETL) through increasing its conductivity. The combined DC sputtered C-TiO_2 and cobalt doped M-TiO_2 has resulted in solar cells efficiencies higher than 16%. It has been found that the C-TiO_2 sputtered at 200 W possess high conductivity and carrier mobility compared to C-TiO_2 sputtered at other DC powers. Moreover, the surface roughness of the C-TiO_2 sputtered at 200 W is almost 38% smaller than the C-TiO_2 prepared at other DC powers. Perovskite material deposited on the optimised C-TiO_2 and cobalt doped M-TiO_2 produced solar cells with higher, J_{sc}, V_{oc}, FF and efficiencies as high as 15.3% in forward and 16.7% at backward scanning. Cells prepared at these conditions have shown good reproducibility and an average drop of 5% in efficiency over 70 days exposure to standard sunlight at room temperature.

Author contribution statement

A. Hayali conceived the original idea, performed the experimental work and wrote draft of the manuscript. M. M. Alkaisi supervised the work, performed analysis and contributed to the discussion of the results, and revised the manuscript.

The authors would like to acknowledge the support of the MacDiarmid Institute for Advanced Materials and Nanotechnology, and thank Linda Chen, Gary Turner and Helen Devereux from the Nanofabrication Laboratory, University of Canterbury, New Zealand for providing technical assistance. Ahmed Hayali acknowledges UC Doctoral Scholarship, University of Canterbury, New Zealand.

References

1. A. Kojima et al., Organometal halide perovskites as visible-light sensitizers for photovoltaic cells, J. Am. Chem. Soc. **131**, 6050 (2009)
2. J. Jeong et al., Pseudo-halide anion engineering for α-$FAPbI_3$ perovskite solar cells, Nature **592**, 381 (2021)
3. N.J. Jeon et al., Solvent engineering for high-performance inorganic-organic hybrid perovskite solar cells, Nat. Mater. **13**, 897 (2014)
4. D. Bi et al., Polymer-templated nucleation and crystal growth of perovskite films for solar cells with efficiency greater than 21%, Nat. Energy **1**, 16142 (2016)
5. F. Bella et al., Improving efficiency and stability of perovskite solar cells with photocurable fluoropolymers, Science **354**, 203 (2016)
6. Y. Wang et al., Solvent annealing of PbI_2 for the high-quality crystallization of perovskite films for solar cells with efficiencies exceeding 18%, Nanoscale **8**, 19654 (2016)
7. D. Bi et al., Facile synthesized organic hole transporting material for perovskite solar cell with efficiency of 19.8%, Nano Energy **23**, 138 (2016)
8. M. Ferreira et al., SnO_2 thin Film Oxides Produced by rf Sputtering for Transparent Thermoelectric Devices, Mater. Today Proc. **2**, 647 (2015)
9. R.D. Chavan et al., Ruthenium doped mesoporous titanium dioxide for highly efficient, hysteresis-free and stable perovskite solar cells, Sol. Energy **186**, 156 (2019)
10. M.C. Wu et al., Enhanced short-circuit current density of perovskite solar cells using Zn-doped TiO_2 as electron transport layer, Sol. Energy Mater. Sol. Cells **157**, 447 (2016)
11. D. Liu et al., Efficient planar heterojunction perovskite solar cells with Li-doped compact TiO_2 layer, Nano Energy **31**, 462 (2017)
12. J.H. Heo et al., Hysteresis-less inverted $CH_3NH_3PbI_3$ planar perovskite hybrid solar cells with 18.1% power conversion efficiency, Energy Environ. Sci. **8**, 1602 (2015)
13. Y. Li et al., Defective TiO_2 with high photoconductive gain for efficient and stable planar heterojunction perovskite solar cells, Nat. Commun. **7**, 12446 (2016)
14. S.S. Mali et al., Efficient planar n-i-p type heterojunction flexible perovskite solar cells with sputtered TiO_2 electron transporting layers, Nanoscale. **9**, 3095 (2017)
15. M. Saliba et al., How to Make over 20% Efficient Perovskite Solar Cells in Regular (n-i-p) and Inverted (p-i-n) Architectures, Chem. Mater. **30**, 4193 (2018)
16. S. Sidhik et al., Improving the Optoelectronic Properties of Mesoporous TiO_2 by Cobalt Doping for High-Performance Hysteresis-free Perovskite Solar Cells, ACS Appl. Mater. Interfaces **10**, 3571 (2018)

17. M.I. Saidaminov et al., High-quality bulk hybrid perovskite single crystals within minutes by inverse temperature crystallization, Nat. Commun. **6**, 7586 (2015)
18. M. Saliba et al., Cesium-containing triple cation perovskite solar cells: Improved stability, reproducibility and high efficiency, Energy Environ. Sci. **9**, 1989 (2016)

Cite this article as: Ahmed Hayali, Maan M. Alkaisi, High efficiency perovskite solar cells using DC sputtered compact TiO_2 electron transport layer, EPJ Photovoltaics **12**, 8 (2021)